Journal of Hazardous Materials 300 (2015) 572–580

Contents lists available at ScienceDirect

Journal of Hazardous Materials

journal homepage: www.elsevier.com/locate/jhazmat

From spent Mg/Al layered double hydroxide to porous carbon materials

Minwang Laipan[a,b], Runliang Zhu[a,*], Qingze Chen[a,b], Jianxi Zhu[a], Yunfei Xi[c], Godwin A. Ayoko[c], Hongping He[a]

[a] Key Laboratory of Mineralogy and Metallogeny, Guangzhou Institute of Geochemistry, Chinese Academy of Sciences, Guangdong Provincial Key Laboratory of Mineral Physics and Material Research & Development, Guangzhou 510640, China
[b] University of Chinese Academy of Sciences, Beijing 100049, China
[c] School of Chemistry, Physics and Mechanical Engineering, Science and Engineering Faculty, Queensland University of Technology, GPO Box 2434, Brisbane, Queensland 4001, Australia

GRAPHICAL ABSTRACT

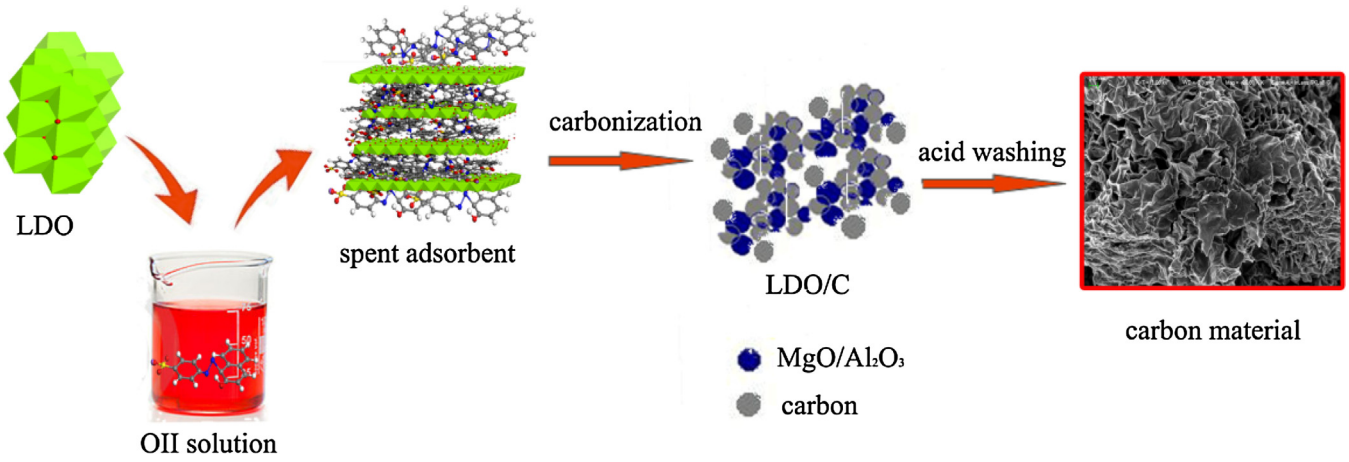

HIGHLIGHTS

- Adsorption properties of Mg/Al-LDH and Mg/Al-LDO toward anionic dye orange II were tested.
- Porous carbon materials were synthesized via in situ method from the spent adsorbent.
- The porous carbon materials possessed of considerable BET specific surface area and pore volume.
- The porous carbon materials exhibited high efficiency in toluene removal.
- The developed resource recycling method proved to be simple, facile and applicable.

ARTICLE INFO

Article history:
Received 6 March 2015
Received in revised form 18 June 2015
Accepted 21 July 2015
Available online 26 July 2015

* Corresponding author. Fax: +86 20 85297603.
E-mail address: zhurl@gig.ac.cn (R. Zhu).

http://dx.doi.org/10.1016/j.jhazmat.2015.07.057

ABSTRACT

Adsorption has been considered as an efficient method for the treatment of dye effluents, but proper disposal of the spent adsorbents is still a challenge. This work attempts to provide a facile method to reutilize the spent Mg/Al layered double hydroxide (Mg/Al-LDH) after the adsorption of orange II (OII). Herein, the spent hybrid was carbonized under the protection of nitrogen, and then washed with acid to obtain porous carbon materials. Thermogravimetric analysis results suggested that the carbonization could be well achieved above 600 °C, as mass loss of the spent hybrid gradually

Keywords:
Calcined layered double hydroxide
Dye effluents treatment
Spent adsorbent recycling
Porous carbon material
Volatile organic compound

stabilized. Therefore, the carbonization process was carried out at 600, 800, and 1000 °C, respectively. Scanning electron microscope showed that the obtained carbon materials possessed a crooked flaky morphology. Nitrogen adsorption–desorption results showed that the carbon materials had large BET surface area and pore volume, e.g., 1426 m^2/g and 1.67 cm^3/g for the sample carbonized at 800 °C. Moreover, the pore structure and surface chemistry compositions were tunable, as they were sensitive to the temperature. Toluene adsorption results demonstrated that the carbon materials had high efficiency in toluene removal. This work provided a facile approach for synthesizing porous carbon materials using spent Mg/Al-LDH.

LDHs Layered double hydroxides
LDOs Layered double oxides
Mg/Al-LDH Mg-Al-CO_3^{2-} layered double hydroxide
Mg/Al-LDO Calcined Mg-Al-CO_3^{2-} layered double hydroxide
OII Orange II
Mg/Al-LDH-OII The hybrid resulted from the adsorption of OII on Mg/Al-LDO
LDO-Carbon The composites of Mg/Al-LDO and carbon obtained from the carbonization product of the spent Mg/Al-LDH without acid washing
LDO-Carbon-600 The composites of Mg/Al-LDO and carbon obtained from the
LDO-Carbon-800 The composites of Mg/Al-LDO and carbon obtained from the
R-LDH The reconstructed product of Mg/Al-LDO in water
Carbon-600 Porous carbon material obtained at 600 °C from the spent Mg/Al-LDH after acid washing
Carbon-800 Porous carbon material obtained at 800 °C from the spent Mg/Al-LDH after acid washing
AC Commercial activated carbon purchased from CARLIME, China
COII-600 The carbonized product of pure OII at 600 °C

1. Introduction

Remnant dyes in the effluents are generally toxic and resistant to biodegradation, which may affect the ecological symbiotic balance of the receiving water stream [1–3]. As such, various methods have been developed for removing dye pollutants, and among them adsorption has drawn particular interests, as it possesses the merits of high-efficiency and simplicity of operation.

Layered double hydroxides (LDHs) have been considered as effective adsorbent for removing anionic dyes from water [4–8]. LDHs have positively charged metal hydroxide sheets with anions located interstitially, and they can efficiently adsorb anionic dyes through an anion exchange process. Moreover, LDHs can be easily and massively synthesized. One of the interesting characteristics of LDHs is that their calcined products, also known as layered double oxides (LDOs), can rehydrate and recover to LDHs in aqueous environment [9]. LDOs therefore can effectively adsorb anionic dyes from wastewater as well. For example, when Mg–Al–CO_3^{2-} LDH is calcined, the CO_3^{2-} could decompose easily. As such, the anionic dye molecules might directly serve as counter ions to balance the positive charge in the reconstruction process. In this case, the spent LDHs can be recycled by calcination treatment after the adsorption of anionic dyes. However, this method also has its drawbacks. For example, copious amounts of carbon dioxide, and some other gases (e.g., SO_2 and/or NO_x) will be released during calcination, which can intensify the greenhouse effect and form secondary pollution. Therefore, new methods for recycling/disposing the spent LDHs should be developed. To address this need, some researchers utilized the LDH/LDO-dyes hybrids as nanofiller or colorant filler for polymer materials [10–12].

Recently, templated synthesis of porous carbon materials using organic compounds-minerals hybrids as a precursor is also drawing increasing interests. In this method, porous carbon materials can be obtained by directly carbonizing the adsorbed organic compounds within the channels of minerals [13,14]. Chen et al. [15] found that carbonizing the spent montmorillonite after the adsorption of cationic dye (crystal violet) could eventually lead to graphene-like carbon materials. Accordingly, carbonizing spent LDH after the adsorption of anionic dyes may generate carbon materials as well, and this could be an efficient method for recycling the spent LDH.

In this work, the spent LDH after the adsorption of anionic dye was carbonized under nitrogen, with the aim of synthesizing porous carbon materials. Orange II (OII) (its chemical formula and structure was shown in Fig. 1) was selected as the representative of anionic dyes, and calcined Mg–Al–CO_3^{2-} layered double hydroxide (i.e., Mg/Al-LDO) was chosen as the adsorbent. Firstly, the adsorption capacity of OII on Mg/Al–LDO was evaluated. Then, the resulting hybrid was carbonized under nitrogen at 600, 800, and 1000 °C, respectively, to generate Mg/Al-LDO–carbon composites (LDO–Carbon). After that, HCl was used to wash out Mg/Al-LDO. The structural characteristics of the resulting carbon materials were investigated using X-ray diffraction (XRD), thermogravimetric analysis (TG), X-ray photoelectron spectroscopy (XPS), scanning electron microscope (SEM), and N_2 adsorption–desorption. The adsorption capacity of the obtained carbon materials toward toluene was further evaluated. The results of this work demonstrated that after the adsorption of OII, LDH could be used to synthesize porous carbon materials.

2. Materials and methods

2.1. Preparation of LDH/LDO

According to our preliminary experimental results, the adsorption capacity of 4:1 (molar ratio of $Mg^{2+}/Al^{3+} = 4$) Mg/Al-LDH toward OII was higher than that of 2:1 and 3:1 Mg/Al-LDH (Fig. S1). As such, we selected 4:1 Mg/Al-LDH as adsorbent, and synthesized using conventional coprecipitation method [16–18]. Firstly, two 300 mL solutions were prepared, one containing 0.24 mol $Mg(NO_3)_2{\cdot}6H_2O$ and 0.06 mol $Al(NO_3)_3{\cdot}9H_2O$, and the other involving 0.5 mol sodium hydroxide and 0.1 mol sodium carbonate. Then, the pre-made solutions were added dropwise into a beaker (containing 150 mL of ultrapure water) under vigorous stirring at room temperature. The pH was maintained at 10 ± 0.2 using an automatic pH controller (Chroma CPH-2, China). The heavy gel was allowed to crystallize by heating at 75 °C for 18 h. After that, the product was centrifuged and washed with ultrapure water until the supernatant pH was below 8, and then dried at 80 °C overnight. The synthetic Mg/Al-LDH had a chemical formula of $[Mg_{0.79}Al_{0.21}(OH)_2](CO_3)_{0.105}{\cdot}0.65H_2O$, which was determined by ICP–MS (Agilent, 7700X) and TG analysis (the dehydration temperature generally

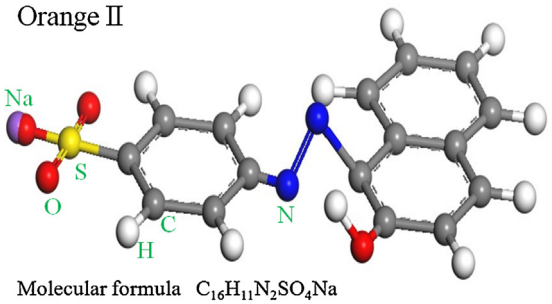

Molecular formula	$C_{16}H_{11}N_2SO_4Na$
Molecular weight	350.32
Width (Å)	7.3
Length (Å)	13.6
Depth (Å)	2.3

Fig. 1. Chemical formula and structure of Orange II.

is around 100–250 °C [19]), and the theoretical calculation value of anionic exchange capacity (AEC) was 272.9 mmol/100 g. Mg/Al-LDO was obtained by heating Mg/Al-LDH at 500 °C for 3 h, and according to the TG analysis result the interlayer carbonate of Mg/Al-LDH was decomposed completely under this temperature.

2.2. Adsorption of OII on LDH and LDO

OII adsorption experiments were carried out by batch adsorption method in a shaker under room temperature (25 °C). About 0.2 g of Mg/Al-LDH or Mg/Al-LDO was dispersed in 50 mL OII solutions of varying concentrations (0.1–8 g/L). After a given contact time for adsorption (12 h), the solid was separated by centrifugation. The supernatant solutions were collected, and then analyzed at 485 nm using a UV–vis spectrophotometer (Perking Elmer Precisely Lambda 850). The OII adsorption results showed that Mg/Al-LDO was more effective than Mg/Al-LDH (Fig. 2), as such Mg/Al-LDO was chosen as the adsorbent for OII removal. It should be pointed out that around the adsorption process, Mg/Al-LDO would revert to LDH structure. In this case, after OII adsorption the resulting hybrid should be named as Mg/Al-LDH-OII rather than Mg/Al-LDO-OII.

2.3. Preparation of carbon materials

Pyrolysis of Mg/Al-LDH-OII hybrid was performed in a tubular furnace under constant nitrogen flow. In detail, the dried Mg/Al-LDH-OII powders (with the adsorbed OII of 1066 mg/g) were loaded to a crucible, and then heated in a temperature-controlled tubular furnace to the required temperature. The heating rate was 2 °C/min, and the samples were maintained at the target temperature for 3 h. The carbonization temperatures (600–1000 °C) were chosen according to the results of TG analysis, as mass loss of Mg/Al-LDH-OII gradually stabilized above 600 °C. The resulting LDO–Carbon composites were washed with HCl (2 M) for 6 h under magnetic stirring to completely remove the inorganic Mg/Al-LDO phase. The carbon materials were further washed several times with ultrapure water, and then dried at 80 °C overnight. The carbon materials obtained at 600, 800, and 1000 °C are herein referred to as Carbon-600, Carbon-800, and Carbon-1000, respectively. For clarity, the meaning of all the abbreviations was given at the end of this article.

2.4. Characterization methods

TG analysis was carried out on a Netzsch STA 490 PC thermal analyzer at a heating rate of 10 °C/min in the temperature range from 30 to 1000 °C. The carbon materials were carried out under air atmosphere; other samples were under nitrogen atmosphere. The flow rate was 60 mL/min. On the other hand, the derivative thermogravimetry (DTG) curves were also utilized in samples analysis.

XRD patterns of the samples were measured on a Bruker D8 ADVANCE X-ray diffractometer using Cu Kα radiation operating at 40 kV and 40 mA. Sample powders were pressed on sample supports, and followed immediately by XRD measurement. The patterns were recorded over the 2θ range from 2 to 70° with a scan speed of 3°/min.

The XPS spectra of the elements in the carbon materials were recorded using a Kα X-ray photoelectron spectrometer (Thermo Fisher Scientific, UK) with a monochromatic Al Kα X-ray source. Binding energies were calibrated using the C 1 s XPS spectra (284.6 eV). The high resolution spectra were analyzed by performing background subtraction and iterative line shape deconvolution, based on a summed Gauss–Lorentz function. In addition, pHpzc of the samples were determined by Zeta potential measurements according to the previous method [20].

The morphology of the samples was recorded by a ZEISS SUPRA 55 SAPPHIRE field-emission scanning electron microscope. The sample powders were firstly stuck to conductive silver adhesives on a glass slide, and then sprayed with a thin layer of conductive carbon to enhance the conductivity before observation.

Nitrogen adsorption–desorption measurements were determined at 77 K using an ASAP 2020 Surface Area & Pore Size Analyzer (Micromeritics Instrument Corporation). Prior to the measurements, the samples were degassed in vacuum at 150 °C for 12 h. Specific surface area was calculated using the Brunauer–Emmett–Teller (BET) method. Total pore volume was determined from the adsorbed amount of nitrogen at $P/P_0 = 0.99$. Pore size distribution and micropore volume were calculated using nonlocal density functional theory (NLDFT) under carbon slit pore model for the adsorption isotherm. In addition, mesopore volume was determined according to BJH method.

2.5. Toluene adsorption experiments

To verify the adsorption properties of the obtained carbon materials, adsorption of toluene was carried out at 25 °C on a dynamic adsorption apparatus (Supplementary materials Fig. S2). The experiments used two gas flows, one is the high purity nitrogen for dilution, and the other is for the target gas (nitrogen as the carrier gas) [21,22]. The total flow maintained at 300 cm^3/min using sensitive mass flow controllers. During the adsorption process, the two gas flows were firstly introduced into a gas mixing chamber wherein the toluene gases were completely diluted. Then the mixture was conducted into the adsorption column where 0.15–0.20 g of adsorbent (stuck by silica wool) was placed. By controlling the flow rates with accurate mass flow controllers, the relative partial pressure of toluene was controlled over a range from 0.08 to 0.99. The toluene adsorption isotherms were determined by gravimetric method, and the adsorption was seen as equilibrium until the variation in the weight was <1 mg for each relative partial pressure. Before the experiment, the adsorbents were degassed at 105 °C for 12 h. For comparison, the LDO–Carbon composites and a commercial activated carbon denoted as AC (from CARLIME, China) with a similar BET specific surface area as the obtained carbon materials were also determined in the toluene adsorption.

3. Results and discussion

3.1. OII adsorption results

Adsorption isotherms of OII on Mg/Al-LDH and Mg/Al-LDO were compared (Fig. 2). The results showed that Mg/Al-LDO was more efficient than Mg/Al-LDH, well in agreement with many other

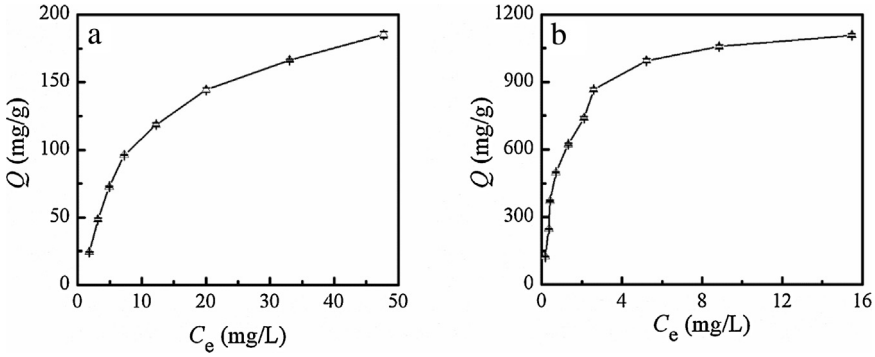

Fig. 2. Adsorption isotherms of orange II on Mg/Al-LDH (a), and Mg/Al-LDO (b) at 25 °C.

studies of anionic dyes adsorption [7,23–25]. In this study, the maximum adsorbed amount of OII on Mg/Al-LDO and Mg/Al-LDH could respectively reach 1066.0 and 475.0 mg/g, which were higher than that on most carbon materials with large specific surface area (842–1488 m^2/g) as reported in literatures [26,27]. As is well known, carbonate has a higher affinity to the positive layers of Mg/Al-LDH than many other anions. In this case, direct exchange of carbonate anions from Mg/Al-LDH by dye anions should be difficult. Conversely, in the case of Mg/Al-LDO, carbonate anions had been eliminated by calcination. As such, during the reconstruction process, dye anions would more easily occupy the charge sites; this was one of the possible reasons for the better adsorption capacity of Mg/Al-LDO. However, we should also notice that when calcinated at 500 °C, Mg/Al-LDH lost about 43.0% of its mass (Fig. S3c), which means that 1 g Mg/Al-LDH could only generate 0.57 g Mg/Al-LDO. As such, OII adsorption capacity on 1 g Mg/Al-LDH probably should be compared to that on 0.57 g Mg/Al-LDO; thus the corresponding adsorption capacity should be 475.0 mg/g for the original Mg/Al-LDH and 607.6 mg/g for the reconstructed Mg/Al-LDH. In this case, the difference of the adsorption capacity on Mg/Al-LDH and LDO was not that much (475–1066 mg/g).

3.2. Thermal analysis results

The TG-DTG curves of Mg/Al-LDH-OII were compared with those of pure OII, and the rehydrated product of Mg/Al-LDO (i.e., R-LDH). The TG curve of R-LDH showed two mass loss steps (Fig. S3), which corresponded to the desorption of water molecules (DTG peak at ~173 °C), and the decomposition of carbonate in combination with the dehydroxylation (DTG peak at ~399 °C), well in agreement with the literature [28]. Through obvious mass lose stages in the heating process, the final mass loss of R-LDH reached 46.6%. In the case of pure OII, mass loss was significant, and continued up to 800 °C with a rapid mass loss appearing between 700 and 800 °C (Fig. S3). Finally, about 51.0% mass loss occurred, which indicated that about 49.0% of OII was transformed into carbonized material. The thermal decomposition characteristics of Mg/Al-LDH-OII were significantly different from those of R-LDH and pure OII, with two major differences (Fig. 3): (1) Liberation of the adsorbed water from Mg/Al-LDH-OII was easier than that from R-LDH. The liberation temperature on the corresponding DTG peaks was approximately 54 °C different, which indicated a weaker interaction between Mg/Al-LDH and water molecules after the loading of OII. Moreover, mass loss of the adsorbed water from Mg/Al-LDH-OII (7.1%) was obviously less than that from R-LDH (16.5%). These results demonstrated that loading of OII could enhance the hydrophobicity. (2) Pure OII had a sharp mass loss (21.8%) in the temperature range from 600 to 800 °C, while the mass loss of Mg/Al-LDH-OII gradually stabilized above 600 °C. Moreover, the final mass loss of Mg/Al-LDH-OII (40.3%) was less than that of both R-LDH (46.5%) and pure OII (51.0%). These results indicated that the thermal stability of OII was enhanced after being adsorbed onto Mg/Al-LDO.

The TG-DTG curves of the obtained carbon materials were plotted as well, which showed that Carbon-600 had higher content and desorption temperature of adsorbed water than Carbon-800 (Fig. 3), indicating Carbon-600 had better affinity to water molecules than Carbon-800. The residual mass of Carbon-600 and Carbon-800 was 1.8% and 6.6% respectively, which indicated that most of the Mg/Al-LDO was washed out by acid. However, the residual mass of Carbon-1000 was 38.2% (Fig. S3), which illustrated the existence of many metallic oxides. The larger residual mass of Carbon-800 and Carbon-1000 indicated that more acid-resistant substances were formed at higher carbonization temperature, and thus higher carbonization temperature should be avoided (e.g., 1000 °C).

3.3. XRD characterization results

The XRD patterns of various samples were recorded (Fig. 4), which showed that Mg/Al-LDH was well crystallized, with a basal spacing of 0.80 nm. Only the characteristic reflections belonging to MgO were shown on Mg/Al-LDO, as well as LDO-Carbon-600. However, when dispersed in water, Mg/Al-LDO could well reconstruct to LDH (shown by the R-LDH pattern), in good agreement with the previous work [9].

Interestingly, when Mg/Al-LDO was dispersed in OII solution, one could find a weak basal reflection at ~3.7°, which should not be attributed to OII or R-LDH. The low-angle XRD patterns of the mechanical mixture of Mg/Al-LDO and OII, and the mixture of R-LDH and OII did not show this reflection as well (Fig. S4). As such,

Table 1
XPS analytic data of Carbon-600, Carbon-800 and AC.

Elements	Carbon-600		Carbon-800		AC	
	Atomic (%)	FWHM (eV)	Atomic (%)	FWHM (eV)	Atomic (%)	FWHM (eV)
C 1 s	90.0	1.5	93.7	1.2	92.6	1.4
O 1 s	6.7	2.8	4.1	2.5	7.4	3.7
S 2 p	0.7	1.4	0.7	1.2	0	–
N 1 s	1.6	2.4	1.5	1.1	0	–

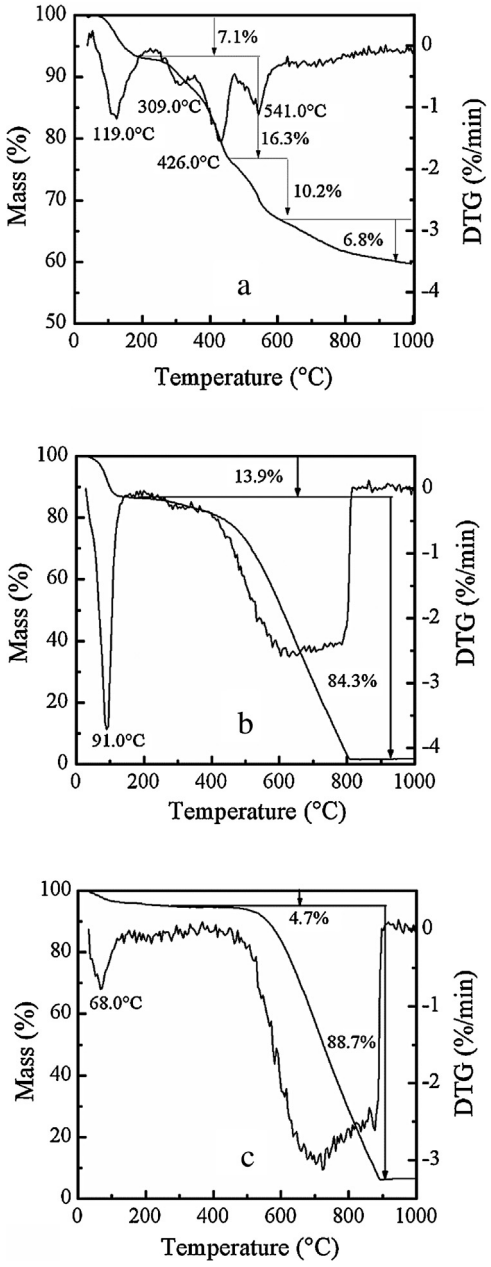

Fig. 3. TG-DTG curves of Mg/Al-LDH-OII (a), Carbon-600 (b), and Carbon-800 (c).

one could conclude that some of the adsorbed OII was successfully intercalated into the interlayers of the reconstructed sample, so the basal spacing was increased to 2.34 nm. Some researchers also found that some other anionic dyes could also be intercalated in the interlayers during the reconstruction process [24,29]. However, one should notice that the charge sites of the reconstructed sample were not completely occupied by OII, according to the AEC of LDH and the adsorbed amount of OII. The AEC of the reconstructed sample from 1 g LDO was theoretically equal to that of ~1.75 g LDH (1 g LDO could generate ~1.75 g LDH in reconstruction). As such, the occupation rate of the charge sites was 63.7% (=1066/(1.75 × 2.729 × 350.32) × 100%) when OII adsorption occurred by taking the charge sites only.

XRD pattern of Carbon-600 presented a weak and broad reflection at 2θ range from 21.0 to 26.0°, indicating amorphous structure of Carbon-600. While two weak reflections (at ~26.0 and 43.0°) corresponding to the characteristic reflections of graphite were shown

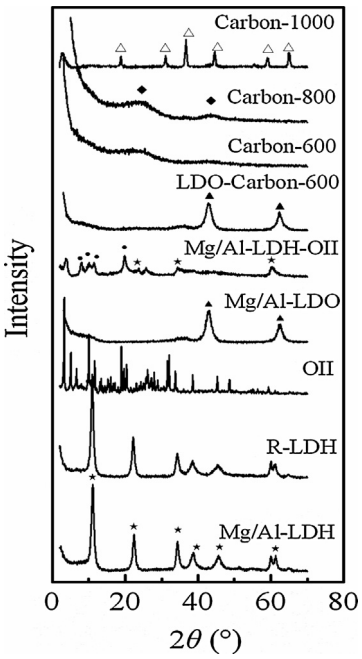

Fig. 4. XRD patterns of Mg/Al-LDH, R-LDH, OII, Mg/Al-LDO, Mg/Al-LDH-OII, Mg/Al-LDO-C (600 °C), Carbon-600, Carbon-800, and Carbon-1000. The reflection peaks labeled with ⋆, ▲, ●, ♦, and △ belong to Mg/Al-LDH, MgO, OII, graphite, and spinel, respectively.

on the XRD pattern of Carbon-800. Mg/Al spinel was formed when the carbonization temperature rose to 1000 °C, which confirmed the forming of acid-resistant substances, well in agreement with the TG-DTG results. Therefore, Carbon-1000 was not utilized in the subsequent experiments.

3.4. XPS characterization results

The XPS survey spectra indicated that the obtained carbon materials contained C, O, S, and N atoms (Fig. S5). With increasing carbonization temperature, the atomic ratio of C increased from 90.0% to 93.7%, and that of O, S, and N decreased (Table 1). This result suggested that Carbon-800 should be more hydrophobic than Carbon-600, consistent with the TG-DTG results. The full width at half maximum (FWHM) of all the atoms was smaller for Carbon-800 (Table 1). Mateos et al. [30] suggested that a smaller FWHM is associated with a better crystallinity of the materials. As such, the C, O, S, and N should have more ordered structure on Carbon-800 than Carbon-600.

The high resolution XPS spectra of C 1 s, S 2 p, and N 1 s of the obtained carbon materials were plotted, and peaks were further deconvolved (Fig. 5). The deconvolution of the C 1 s spectra could yield four peaks, which were assigned to graphitized carbon (284.6 eV) [31–33], amorphous carbon (285.0 eV) [34], C—O—/C=N groups (~286.1 eV) [31,32,35], and C=O/C—N groups (~287.3 eV) [31,32,35]. From the relative contents of the functional groups in C 1 s (Table S1), one could tell that the relative content of the graphitic carbon increased (i.e., from 28.7% to 54.6%), while that of the amorphous carbon decreased (i.e., from 50.3% to 30.9%) from 600 to 800 °C, well in agreement with the XRD results. The decrease of C—O— and C=O/C—N could enhance the hydrophobic characteristic of the carbon materials.

Deconvolution of the S 2 p spectra yielded four peaks as well, corresponding to thiophenol/thiol (PhSH/RSH) (S $2p_{3/2}$ and S $2p_{1/2}$ at ~163.7 and 164.9 eV), and $R_2S=O/SO_3^{2-}$ (S $2p_{3/2}$ and S $2p_{1/2}$ at ~167.8 and 169.5 eV) [35,36]. The relative content of PhSH/RSH was shown to increase slightly with rising carbonization

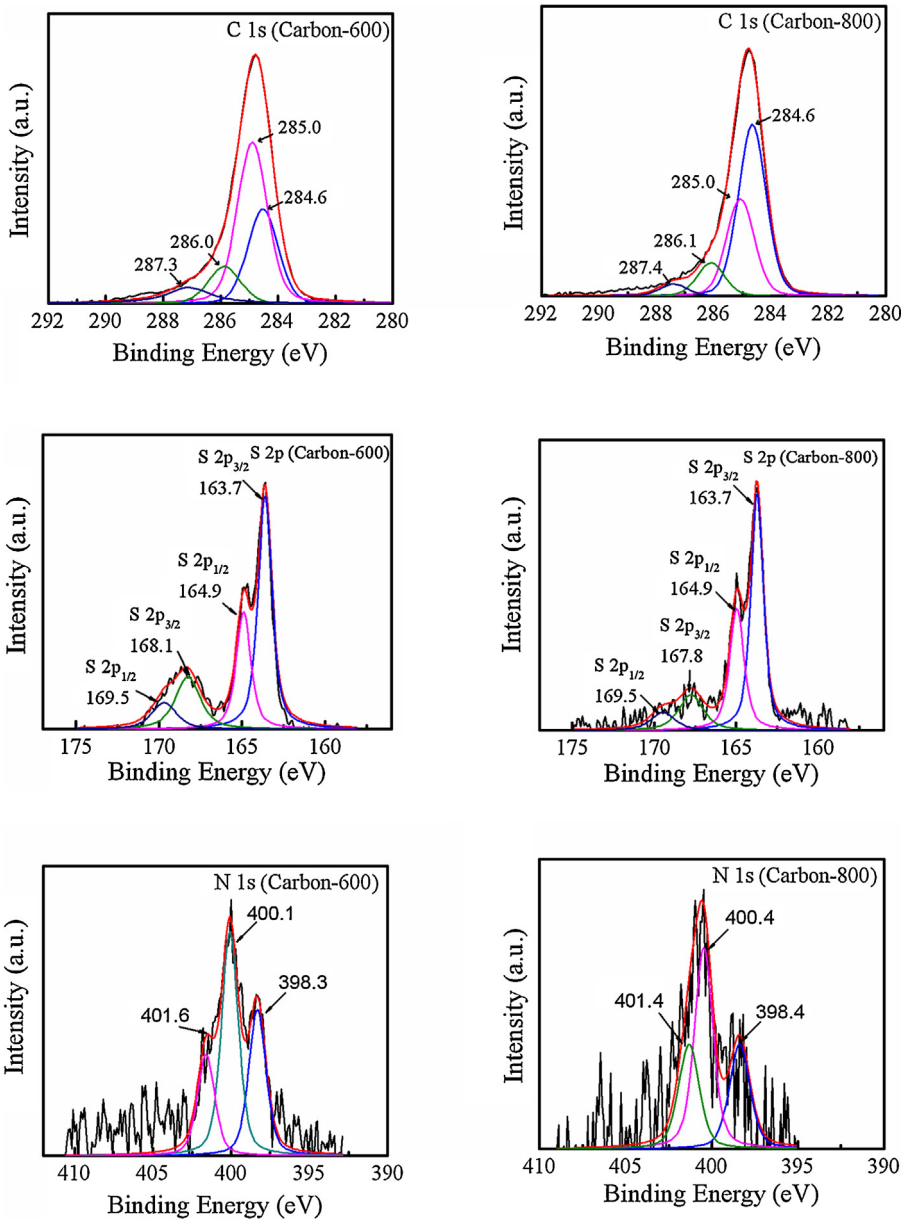

Fig. 5. C 1 s, S 2 p, and N 1 s XPS spectra of Carbon-600 and Carbon-800.

temperature, while that of the $R_2S{=}O/SO_3^{2-}$ decreased (Table S1). Namely, the relative content of oxygen-containing hydrophilic groups decreased, which indicated a better hydrophobicity for Carbon-800 than Carbon-600. Deconvolution of the N 1 s spectra mainly yield three peaks, which could be identified as C—N—C (sp^2 hybridization form) (~398.3 eV) [37], C—N—C (other hybridization forms) (~400.1 eV) [35,38], and C—N^+H—C (~401.4 eV) [35,38]. The binding forms of N atom presented mainly as C—N—C forms (sp^2 and other hybridization forms), and showed no clear change in the relative content among all the N-containing groups with the increase of carbonization temperature from 600 to 800 °C (Table S1). From the above, the surface chemistry compositions of the obtained carbon materials could be adjusted by applying different carbonization temperatures.

As for commercial AC, its surface chemical composition was simpler as compared with Carbon-600 and Carbon-800. According to the XPS survey spectrum (Fig. S5), AC was composed by C and O element, with atomic ratio of 92.6% and 7.4% (Table 1), respectively. The deconvolution of high resolution XPS spectrum of O 1 s showed that AC mainly consisted of C=O (48.1%, ~531.9 eV), C—O— (45.2%, ~533.2 eV) and C=O (6.7%, occluded CO or CO_2, ~536.3 eV) [39] functional groups (Fig. S6a). In addition, according to C 1 s spectrum (Fig. S6b), the C=O and C—O—was attributed to carbonyl/quinone and phenolic/alcoholic/etheric, respectively [39,40].

In addition, the pHpzc values of Carbon-600, Carbon-800, and AC were 7.17, 7.34, and 7.75, respectively (Table 2), indicating a close amount of acidic and basic functional groups or negative and positive charges on each sample.

3.5. Surface morphology and porous structure of the carbon materials

As previously mentioned, some of the OII was intercalated into the interlayers of Mg/Al-LDH-OII, and thus when the layers were destructed during the carbonization process, the carbonized products in the interlayers should form a lamellar structure. XRD and

Table 2
Porosity characterization results and pHpzc of the samples.

Sample	S_{BET} (m^2/g)	V_{total} (cm^3/g)	V_{meso} (cm^3/g)	$V_{(<0.67nm)}$ (cm^3/g)	$V_{(0.67\text{-}0.9nm)}$ (cm^3/g)	$V_{(0.9\text{-}2nm)}$ (cm^3/g)	pHpzc
Carbon-600	1462	0.98	0.34	0.13	0	0.35	7.17
Carbon-800	1426	1.67	1.54	0.06	0	0.22	7.34
AC	1338	0.61	0.12	0.15	0.05	0.26	7.75
C_{OII}-600	0.15	0.01	–	–	–	–	–
LDO-Carbon-600	286	0.25	0.15	–	–	–	–
LDO-Carbon-800	316	0.29	0.20	–	–	–	–

XPS results showed that the obtained carbon materials were partially graphitized, suggesting the carbon materials should possess some lamellar structure. As expected, SEM images demonstrated that both Carbon-600 and Carbon-800 exhibited a curly lamellar structure (Fig. 6). However, unlike the rigid lamellar structure of the precursor of Mg/Al-LDO (Fig. S7), the lamellas of the obtained carbon materials were bending at random direction, which could result in large porosity and slit pores.

The N_2 adsorption–desorption isotherms of the obtained carbon materials were compared with that of commercial active carbon AC. All of the obtained isotherms showed a steep increase of N_2 adsorbed amounts at low relative pressure range, indicating these carbon materials all contained large amount of micropores (Fig. 7). Some differences, however, could be clearly observed among Carbon-600, Carbon-800, and AC. The adsorption-desorption isotherm of AC contained a plateau, and a nearly negligible hysteresis loop. As such, the isotherm could be classified as type I, indicating that AC was mostly comprised of micropores. However, the isotherms of the obtained carbon materials revealed some type I and IV characters, as they presented a pronounced hysteresis loop and a slope with the increase of relative pressures. These results indicated that the obtained carbon materials simultaneously contained large amount of micropores and mesopores. The H4 desorption hysteresis suggested that the obtained carbon materials contained mainly slit pores, but some of the pores of Carbon-800 might deform to other forms, as the "paunch" of the hysteresis loop expanded. The adsorbed amounts of N_2 on the obtained carbon materials were lower than that on AC at low relative pressure range, with an order AC > Carbon-600 > Carbon-800, while converse results were obtained at higher relative pressure range.

The calculated BET specific surface areas and pore volumes of the samples were listed in Table 2. Both Carbon-600 and Carbon-800 had large BET specific surface area and high total pore volume. However they had a pronounced difference in mesopore volume with 0.34 and 1.54 cm^3/g for Carbon-600 and Carbon-800, respectively. Combination with the result on the pore size distribution, one could clearly tell that Carbon-600 contained mainly micropores with a pore size range from 0.5 to 2.0 nm. However, Carbon-800 mostly comprised of mesopores with a wider pore size range mainly from 1.0 to 12.0 nm (Fig. 7). As such, more mesopores were created with increasing carbonization temperature, and thus resulted in higher mesopore volume. In this case, pore type, pore volume, and pore size distribution were tunable, as they were sensitive to the temperature.

For comparison, pore structure of the carbonized product of pure OII at 600 °C (C_{OII}-600) and the Mg/Al-LDO-carbon composites obtained under 600 and 800 °C, namely LDO-Carbon-600 and LDO-Carbon-800, were measured as well (Table 2). The result showed that C_{OII}-600 presented only a small specific surface area

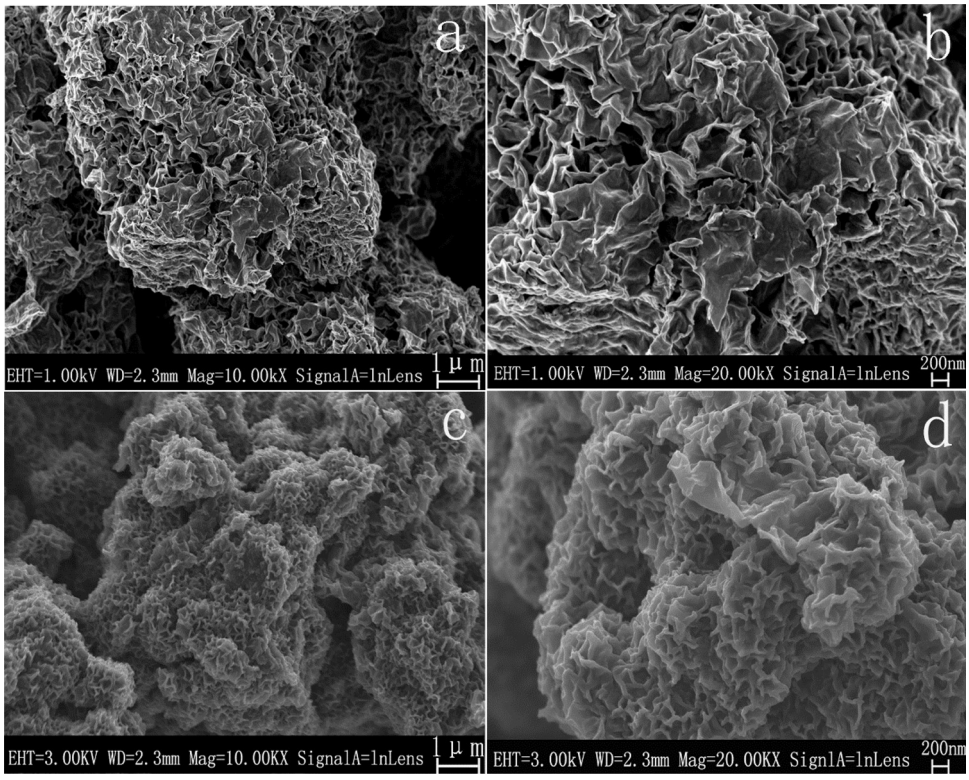

Fig. 6. SEM images of Carbon-600 (a, b) and Carbon-800 (c, d).

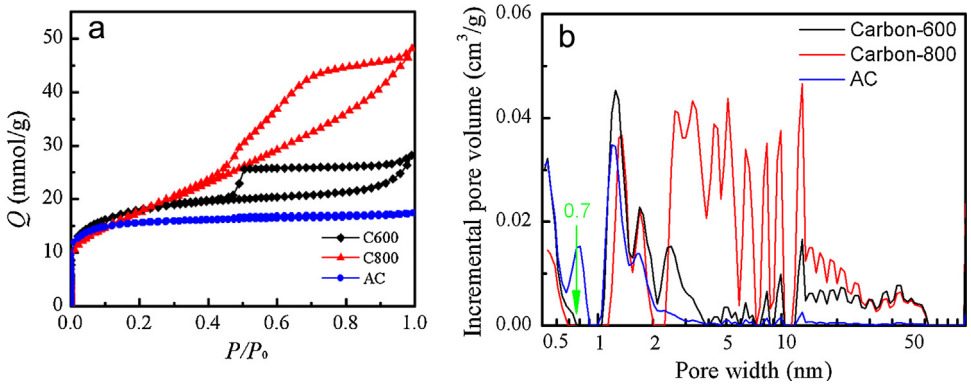

Fig. 7. N_2 adsorption-desorption isotherms (a) and NLDFT pore size distribution (b) of Carbon-600, Carbon-800, and AC.

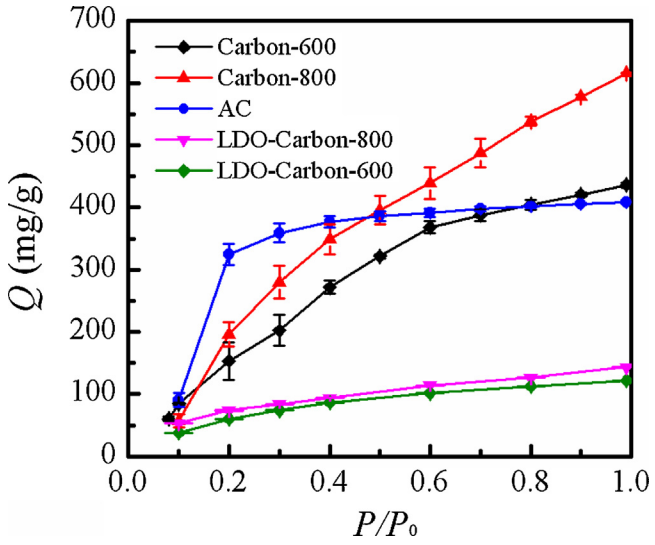

Fig. 8. Toluene adsorption isotherms on Carbon-600, Carbon-800 and AC.

(0.15 m^2/g), and total pore volume (0.01 cm^3/g). As such, the large BET specific surface area and high pore volume of the obtained carbon materials should be ascribed to the template effect of Mg/Al-LDO.

3.6. Toluene adsorption properties of the carbon materials

As the obtained carbon materials possessed large specific surface areas and high pore volumes, they may have attractive applications in many fields, e.g., adsorption of organic contaminants. Toluene adsorption results showed that the obtained carbon materials had better adsorption capacity than LDO-Carbon composites (Fig. 8), with the maximum adsorbed amount of 436.2 mg/g on Carbon-600 and 615.6 mg/g on Carbon-800, several times larger than that on LDO-Carbon-600 (121.5 mg/g) and LDO-Carbon-800 (143.5 mg/g). As for AC, it also presented a high adsorption capacity with a maximum adsorbed amount of 402.0 mg/g. However, its adsorption isotherm was significantly different from those of the obtained carbon materials. In particular, the adsorption of toluene on AC mainly occurred in low relative pressure range; while the adsorption on the obtained carbon materials showed continual increase with the rise of relative pressure.

The adsorption of contaminants on adsorbents mainly depends on two factors: (1) the available adsorption sites/volume and (2) the sorbate–sorbent interaction affinity [41]. As Carbon-600 had slightly larger volume of micropores of 0.67–2 nm (0.35 cm^3/g; 0.67 nm, the molecular size of toluene [42]) than that of AC (0.31 cm^3/g) (Table 2), theoretically Carbon-600 should have a better adsorption capacity in low relative pressure range. However, the adsorption isotherms clearly showed reverse results, which might partly be attributed to the difference of pore shapes on these adsorbents. Considering the pore type of the obtained carbon materials was mainly slit pores (determined from N_2 adsorption, and also suggested by the SEM results), the available micropore volume for toluene might be less than the volume determined from N_2 adsorption (as molecule size of toluene was larger than that of N_2). In addition, the lack of pores with sizes of 0.67–0.9 nm (close to the molecule size of toluene) on the obtained carbon materials (Fig. 7) might be another reason.

On the other hand, the surface functional groups of the obtained carbon materials (C═O, C—O—, —SH, —S═O/SO_3^{2-}, C–N^+H–C, etc.) were more complex than that of AC (mainly C═O and C—O—), according to XPS analysis. As we know, the specific interaction between π-electron rich regions of the carbon layers and aromatic rings was one of the important sorbate-sorbent interactions [43–46]. Lillo-Rodénas et al., pointed out that surface functional groups on carbon materials could affect π-electron rich regions of the carbon layers, and thus weaken the specific interactions between π-electron rich regions of the carbon layers and the aromatic rings of aromatic compounds [47]. As such, the presence of complex surface groups on the obtained carbon materials might have some negative effect on the interaction between toluene and the obtained carbon materials, leading to relatively weaker adsorption capacity.

At relatively high pressure, the isotherm of AC exhibited a plateau with toluene adsorbed amount increasing only slightly. However, the isotherms showed that the adsorbed amounts on the obtained carbons increased continually. This might be attributed to the mesoporosity adsorption or the adsorbate–adsorbate interaction [41].

4. Conclusions

The present study showed that Mg/Al-LDO could effectively remove anionic dye OII from water, and OII could intercalate into the interlayers of the reconstructed Mg/Al-LDH showing an increased basal spacing of 2.34 nm. The spent adsorbent could be utilized to obtained carbon materials through carbonizing and acid washing. The obtained carbon materials could be partially graphitized, and had curly lamellar morphology with large BET specific surface areas and high pore volumes. In addition, the surface hydrophobicity, surface chemistry compositions, and pore structure of the obtained carbon materials were tunable by varying the carbonization temperature. Toluene adsorption results illustrated that the obtained carbon materials exhibited much higher maximum adsorbed amount than the commercial activated

carbon, while there is still room for improvement in the low relative pressure range. The results of this work demonstrate that synthesizing porous carbon materials are a promising method for recycling the spent Mg/Al-LDH after the treatment of dye effluents.

Acknowledgment

This work was financially supported by the "One Hundred Talents program" of the Chinese Academy of Sciences (KZZD-EW-TZ-10), grants from the National Natural Science Foundation of China (41322014, 21177104), Team Project of Natural Science Foundation of Guangdong Province (S2013030014241), and CAS/SAFEA International Partnership Program for Creative Research Teams (20140491534). This is contribution No. IS - 2104 from GIG CAS. Finally, we would like to thank the editor Prof. Andrew Daugulis and the reviewers for their valuable comments and warm work.

Appendix A. Supplementary data

Supplementary data associated with this article can be found, in the online version, at http://dx.doi.org/10.1016/j.jhazmat.2015.07.057

References

[1] G. McMullan, C. Meehan, A. Conneely, N. Kirby, T. Robinson, P. Nigam, I.M. Banat, R. Marchant, W.F. Smyth, Microbial decolourisation and degradation of textile dyes, Appl. Microbiol. Biotechnol. 56 (2001) 81–87.
[2] A.K. Mittal, S.K. Gupta, Biosorption of cationic dyes by dead macro fungus fomitopsis carnea: batch studies, Water Sci. Technol. 34 (1996) 81–87.
[3] N.D. Lourenco, J.M. Novais, H.M. Pinheiro, Effect of some operational parameters on textile dye biodegradation in a sequential batch reactor, J. Biotechnol. 89 (2011) 163–174.
[4] A.R. Auxilio, P.C. Andrews, P.C. Junk, L. Spiccia, D. Neumann, W. Raverty, N. Vanderhoek, Adsorption and intercalation of acid blue 9 on Mg–Al layered double hydroxides of variable metal composition, Polyhedron 26 (2007) 3479–3490.
[5] K. Morimoto, K. Tamura, N. Iyi, J. Ye, H. Yamada, Adsorption and photodegradation properties of anionic dyes by layered double hydroxides, J. Phys. Chem. Solids 72 (2011) 1037–1045.
[6] I.M. Ahmed, M.S. Gasser, Adsorption study of anionic reactive dye from aqueous solution to Mg–Fe–CO_3 layered double hydroxide (LDH), Appl. Surf. Sci. 259 (2012) 650–656.
[7] H. Zaghouane-Boudiaf, M. Boutahala, L. Arab, Removal of methyl orange from aqueous solution by uncalcined and calcined MgNiAl layered double hydroxides (LDHs), Chem. Eng. J. 187 (2012) 142–149.
[8] P. Zhang, G. Qian, H. Shi, X. Ruan, J. Yang, R.L. Frost, Mechanism of interaction of hydrocalumites (Ca/Al-LDH) with methyl orange and acidic scarlet GR, J. Colloid Interface Sci. 365 (2012) 110–116.
[9] S. Miyata, Physico-chemical properties of synthetic hydrotalcites in relation to composition, Clays Clay Miner. 28 (1980) 50–56.
[10] Y.-P. Wei, D.-Q. Wei, H.-W. Gao, Treatment of dye wastewater by in situ hybridization with Mg–Al layered double hydroxides and reuse of dye sludge, Chem. Eng. J. 172 (2011) 872–878.
[11] Y.-P. Wei, T. Li, H.-W. Gao, Synthetic dye-inorganic salt hybrid colorants for application in thermoplastics, Molecules 16 (2011) 5035–5053.
[12] T. Xue, Y. Gao, Z. Zhang, A. Umar, X. Yan, X. Zhang, Z. Guo, Q. Wang, Adsorption of acid red from dye wastewater by Zn2Al-NO3 LDHs and the resource of adsorbent sludge as nanofiller for polypropylene, J. Alloys Compd. 587 (2014) 99–104.
[13] D. Gournis, V. Georgakilas, M.A. Karakassides, T. Bakas, K. Kordatos, M. Prato, M. Fanti, F. Zerbetto, Incorporation of fullerene derivatives into smectite clays: a new family of organic-inorganic nanocomposites, J. Am. Chem. Soc. 126 (2004) 8561–8568.
[14] D. Gournis, L. Jankovic, E. Maccallini, D. Benne, P. Rudolf, J.-F. Colomer, C. Sooambar, V. Georgakilas, M. Prato, M. Fanti, F. Zerbetto, G.H. Sarova, D.M. Guld, Clay-fulleropyrrolidine nanocomposites, J. Am. Chem. Soc. 128 (2006) 6154–6163.
[15] Q. Chen, R. Zhu, W. Deng, Y. Xu, J. Zhu, Q. Tao, H. He, From used montmorillonite to carbon monolayer–montmorillonite nanocomposites, Appl. Clay Sci. (2014).
[16] W.T. Reichle, Catalytic reactions by thermally activated, synthetic, anionic clay minerals, J. Catal. 94 (1985) 547–557.
[17] H.-P. Boehm, J. Steinle, C. Vieweger, $[Zn_2Cr(OH)_6]X{\cdot}2H_2O$, New layer compounds capable of anion exchange and intracrystalline swelling, Angew. Chem. Int. Ed. Engl. 16 (1977) 265–266.
[18] W.T. Reichle, Synthesis of anionic clay minerals (mixed metal hydroxides, hydrotalcite), Solid State Ionics 22 (1986) 135–141.
[19] Z.P. Xu, J. Zhang, M.O. Adebajo, H. Zhang, C.H. Zhou, Catalytic applications of layered double hydroxides and derivatives, Appl. Clay Sci. 53 (2011) 139–150.
[20] P. Chingombe, B. Saha, R.J. Wakeman, Surface modification and characterisation of a coal-based activated carbon, carbon 43 (2005) 3132–3143.
[21] L. Zhu, S. Tian, Y. Shi, Adsorption of volatile organic compounds onto porous clay heterostructures based on spent organobentonites, Clays Clay Miner. 53 (2005) 123–136.
[22] F. Qu, L. Zhu, K. Yang, Adsorption behaviors of volatile organic compounds (VOCs) on porous clay heterostructures (PCH), J. Hazard. Mater 170 (2009) 7–12.
[23] M.X. Zhu, Y.P. Li, M. Xie, H.Z. Xin, Sorption of an anionic dye by uncalcined and calcined layered double hydroxides: a case study, J. Hazard. Mater 120 (2005) 163–171.
[24] N. Drici Setti, N. Jouini, Z. Derriche, Sorption study of an anionic dye –benzopurpurine 4B –on calcined and uncalcined Mg–Al layered double hydroxides, J. Phys. Chem. Solids 71 (2010) 556–559.
[25] R.M.M. dos Santos, R.G.L. Gonçalves, V.R.L. Constantino, L.M. da Costa, L.H.M. da Silva, J. Tronto, F.G. Pinto, Removal of acid green 68:1 from aqueous solutions by calcined and uncalcined layered double hydroxides, Appl. Clay Sci. 80-81 (2013) 189–195.
[26] C. Hsiu-Mei, C. Ting-Chien, P. San-De, C. Hung-Lung, Adsorption characteristics of Orange II and Chrysophenine on sludge adsorbent and activated carbon fibers, J. Hazard. Mater. 161 (2009) 1384–1390.
[27] A. Rodriguez, J. Garcia, G. Ovejero, M. Mestanza, Adsorption of anionic and cationic dyes on activated carbon from aqueous solutions: equilibrium and kinetics, J. Hazard. Mater. 172 (2009) 1311–1320.
[28] S.K. Yun, T.J. Pinnavaia, Water Content and particle texture of synthetic hydrotalcite-like layered double hydroxides, Chem. Mater. 7 (1995) 348–354.
[29] R. Extremera, I. Pavlovic, M.R. Pérez, C. Barriga, Removal of acid orange 10 by calcined Mg/Al layered double hydroxides from water and recovery of the adsorbed dye, Chem. Eng. J. 213 (2012) 392–400.
[30] J.M.J. Mateos, J.L.G. Fierro, X-ray photoelectron spectroscopic study of petroleum fuel cokes, Surf. Interface Anal. 24 (1996) 223–236.
[31] J.H. Zhou, Z.J. Sui, J. Zhu, P. Li, D. Chen, Y.C. Dai, W.K. Yuan, Characterization of surface oxygen complexes on carbon nanofibers by TPD, XPS and FT-IR, Carbon 45 (2007) 785–796.
[32] M. Polovina, B. Babic, B. Kaluderovic, A. Dekanski, Surface characterization of oxidized activated carbon cloth, carbon 35 (1997) 1047–1052.
[33] H. Darmstadt, C. Roy, S. Kaliaguine, Characterization of pyrolytic carbon blacks from commercial tire pyrolysis plants, carbon 33 (1995) 1449–1455.
[34] J.C. Lascovich, R. Giorgi, S. Scaglione, Evalution of the sp^2/sp^3 ratio in amorphous carbon structure by XPS and XAES, Appl. Surf. Sci. 47 (1991) 17–21.
[35] A.P. Terzyk, The influence of activated carbon surface chemical composition on the adsorption of acetaminophen (paracetamol) in vitro, Colloid Surf. A-Physicochem. Eng. Asp 177 (2001) 23–45.
[36] U. Zielke, K.J. Huttinger, W.P. Hoffman, Surface-oxidized carbon fibers: I. surface structure and chemistry, Carbon 34 (1996) 983–998.
[37] X. Li, J. Zhang, L. Shen, Y. Ma, W. Lei, Q. Cui, G. Zou, Preparation and characterization of graphitic carbon nitride through pyrolysis of melamine, Appl. Phys. A 94 (2008) 387–392.
[38] J.R. Pels, F. Kapteijn, J.A. Moulijn, Q. Zhu, K.M. Thomas, Evolution of nitrogen functionalities in carbonaceous materials during pyrolysis, carbon 33 (1995) 1641–1653.
[39] T. Karanfil, J.E. Kilduff, Role of granular activated carbon surface chemistry on the adsorption of organic compounds. 1. Priority pollutants, Environ. Sci. Technol. 33 (1999) 3217–3224.
[40] T. Garcia, R. Murillo, D. Cazorla-Amoros, A.M. Mastral, A. Linares-Solano, Role of the activated carbon surface chemistry in the adsorption of phenanthrene, carbon 42 (2004) 1683–1689.
[41] R.T. Yang, Adsorbents: Fundamentals and Applications, John Wiley & Sons, 2003.
[42] M.E. Ramos, P.R. Bonelli, A.L. Cukierman, M.M.L.R. Carrott, P.J.M. Carrott, Adsorption of volatile organic compounds onto activated carbon cloths derived from a novel regenerated cellulosic precursor, J. Hazard. Mater. 177 (2010) 175–182.
[43] R.Q. Long, R.T. Yang, Carbon nanotubes as superior sorbent for dioxin removal, J. Am. Chem. Soc. 123 (2001) 2058–2059.
[44] X.J. Peng, Y.H. Li, Z.K. Luan, Z.C. Di, H.Y. Wang, B.H. Tian, Z.P. Jia, Adsorption of 1,2-dichlorobenzene from water to carbon nanotubes, Chem. Phys. Lett. 376 (2003) 154–158.
[45] S.B. Fagan, A.G. Souza, J.O.G. Lima, J. Mendes, O.P. Ferreira, I.O. Mazali, O.L. Alves, M.S. Dresselhaus, 1,2-dichlorobenzene interacting with carbon nanotubes, Nano. Lett. 4 (2004) 1285–1288.
[46] L.L. Ji, Y. Shao, Z.Y. Xu, S.R. Zheng, D.Q. Zhu, Adsorption of monoaromatic compounds and pharmaceutical antibiotics on carbon nanotubes activated by KOH Etching, Environ. Sci. Technol. 44 (2010) 6429–6436.
[47] M.A. Lillo-Rodenas, D. Cazorla-Amoros, A. Linares-Solano, Behaviour of activated carbons with different pore size distributions and surface oxygen groups for benzene and toluene adsorption at low concentrations, carbon 43 (2005) 1758–1767.